Original Research

Simulated Study on the Degradation of Mono- and Bi-Component Dye Wastewater by TiO$_2$/H$_3$PW$_{12}$O$_{40}$ Film Excited under Solar-Like Radiation

N Lu, YQ Wang, M Luo, J Qu, JN Guan*, X Yuan**

School of Environment, Northeast Normal University, Changchun, P. R. China

Abstract

The objective of this work was to develop an effective technique for removing multiple component dye wastewater. Saturation Keggin-type phosphotungstic acid (H$_3$PW$_{12}$O$_{40}$) was introduced to prepare TiO$_2$/H$_3$PW$_{12}$O$_{40}$ film for photocatalytic degradation of four monocomponent dye wastewater as rhodamine B (RhB), methyl orange (MO), malachite green (MG), and alizarin red (ARS), as well as bicomponent dye wastewater of RhB-MG with different volume ratio. The results indicated that the photocatalytic efficiency of TiO$_2$/H$_3$PW$_{12}$O$_{40}$ film toward cation dyes (98.5% RhB and 95.2% MG) was higher than that of anion dyes (89.8% ARS and 48.8% MO) after 240 min solar-like irradiation, during which the adsorption acted as the controlling process, whereas in the bicomponent dye solution of RhB-MG, the degradation RhB was restrained due to the competition for the active sites of catalyst surface with MG. This work could provide necessary information for the treatment of multiple component dye wastewater in practical applications.

Keywords: dye wastewater, TiO$_2$/H$_3$PW$_{12}$O$_{40}$, photocatalytic degradation, adsorption, bicomponent

Introduction

With the rapid development of industrialization and urbanization, dye wastewater has contributed up to 20% of global wastewater, causing serious environmental issues due to their properties of persistence and toxicity [1-4]. Consequently, a number of approaches have been developed to treat dye wastewater, such as electro-oxidation, ozonating, ion-exchange, membrane filtration, microbial degradation, etc. [5-7]. However, these techniques are either costly or inefficient. Recently the photocatalytic process has been developed to degrade the organic pollutants completely or generate harmless compounds with the aid of a light source, and it has been proven that it is an efficient way to mineralize a variety of dyes in wastewater with a limited cost [8-10].

TiO$_2$ was known as an excellent photocatalyst that can be excited to generate electron/hole pairs under light illumination (UV or solar), producing a strong oxidant of ·OH at its surface with an excellent degrading ability

*e-mail: guanjn461@nenu.edu.cn
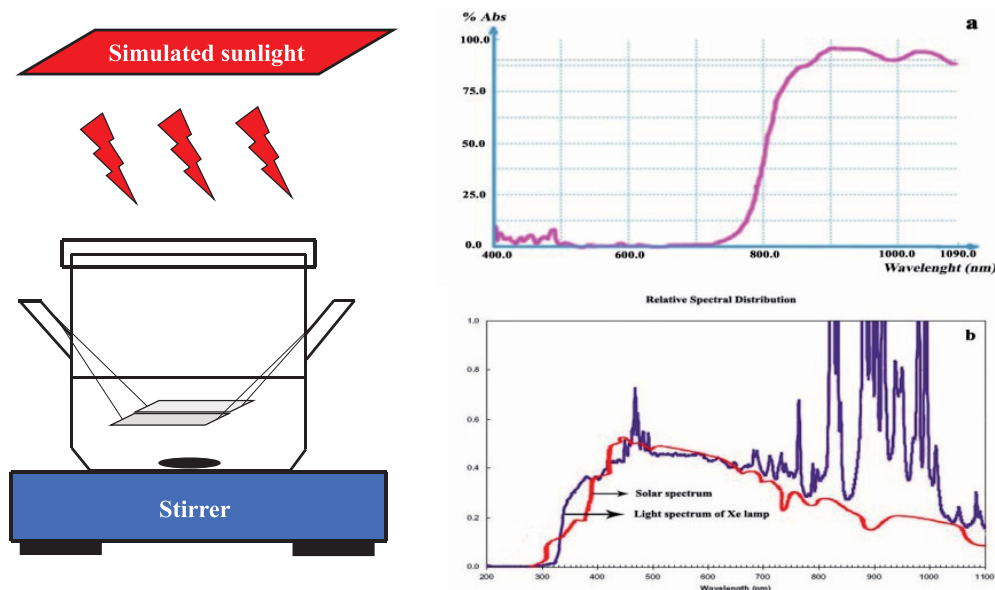**e-mail: yuanx@nenu.edu.cn

Fig. 1. Self-designed quartz reactor. Inset: a) Infrared filter spectrum, b) Xenon lamp (purple) and sunlight (red) spectrum.

Table 1. LD50 values of the dyes

Dye type	Tested organisms	LD50 (mg/kg)
RhB	Rats	89.5
MO	Rats	60.0
ARS	Rats	70.0
MG	Rats	275.0

toward most organic pollution [11]. Heteropolyacid (HPA), which possessed unoccupied W 5d orbit, could capture quickly the electrons of TiO_2's conduction band in order to overcome the drawbacks of TiO_2 (i.e., recombination of the generated electron and hole).

The photocatalytic synergistic effects between HPA and TiO_2 have been confirmed toward different dye wastewater [12]. In addition, due to the unique pseudo-liquid phase structure of HPA, dye solution could flow through in the catalysts, resulting in sufficient contact between dye molecules and active sites on the catalysts [13]. Therefore, HPA-TiO_2 catalyst is an ideal candidate for the removal of dye wastewater.

Currently, research on the photocatalytic degradation of organic pollutants are commonly based on a monocomponent solution focusing on optimizing its effectiveness, including catalyst loadings, calcination temperature, morphology, solution pH, initial concentration, etc. [14-18]. However, the practical dye wastewater usually contains multiple dyes with different structures and physiochemical properties
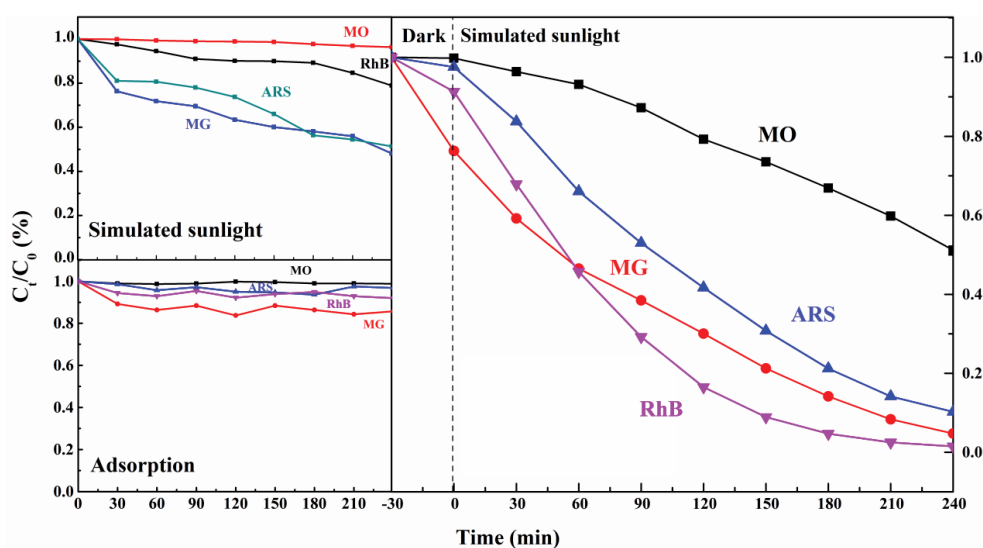

Fig. 2. Direct photolysis of RhB, MO, ARS, and MG, and their adsorption and photocatalytic degradation on $TiO_2/H_3PW_{12}O_{40}$ film.

Table 2 Comparison of RhB, MO, MG, and ARS degradation utilizing various catalysts

Catalysts	Dyes	Irradiation	Percentage	Reference
CdS nanoring 10 mg	RhB 50 ml 1.0×10^{-5} mol·L^{-1}	300 min 55 W fluorescent lamp Visible light	70%	[24]
Bi$_2$MoO$_6$/g-C$_3$N$_4$ 50 mg	RhB 50 ml 1.0×10^{-5} mol·L^{-1}	360 min 300 W Xenon lamp Visible light	72%	[25]
Gd-TiO$_2$ 10 mg	RhB 10 ml 1.0×10^{-5} mol·L^{-1}	240 min 400 W halogen lamp Visible light	93%	[26]
[Ag$_3$L$_4$(PMo$_{12}$O$_{40}$) (CH$_3$OH)]_CH$_3$OH 2.1 mg	RhB 30 ml 2.0×10^{-5} mol·L^{-1}	450 min 500 W mercury lamp Ultraviolet light	62%	[27]
ZnO-graphene 100 mg	RhB 100 ml 1.0×10^{-5} mol·L^{-1}	180 min 8 W Xenon lamp Visible light	71%	[28]
SnS$_2$/TiO$_2$ 100 mg	MO 25 ml 4×10^{-5} M	50 min 200 W Xe arc lamp Simulated sunlight	91%	[29]
ZnO nano-mushrooms 200 mg	MO 100 ml 1.5×10^{-5} M	210 min 36 W high pressure mercury lamp Ultraviolet light	92%	[30]
Cu$_2$S-Cu-TiO$_2$ 120 mg	MO 200 ml 300 mg·L^{-1}	120 min High-pressure sodium lamp Visible light	94%	[31]
TiO$_2$/D-PVA 500 mg	MO 200 ml 10 mg·L^{-1}	40 h 200 W dysprosium lamp Visible light	84%	[32]
La$_{0.7}$Sr$_{0.3}$MnO$_3$ 20 mg	MO 100 ml 13 mg·L^{-1}	20 min Sunlight Sunny days in July 2013 between 10.30 am and 2.00 pm	96%	[33]
Pt-TiO$_2$/SiO$_2$ 200 mg	MG 200 ml 10 mg·L^{-1}	45 min 300 W tungsten lamp Visible light	99%	[34]
Pd/WO$_3$ 50 mg	MG 30 ml 5.0 µmol·L^{-1}	360 min A simulated solar lamp Visible light	90%	[35]
ZnO 20 mg	MG 100 ml 200 mg·L^{-1}	100 min 300 W mercury lamp Ultraviolet light	85%	[36]
CeO$_2$/CdO 30 mg	MG 100 ml 50 mg·L^{-1}	60 min 300 W powder Ultraviolet light	99%	[37]
(NH$_4$)$_3$[PW$_{12}$O$_{40}$] 24 mg	MG 40 ml 10 µM	40 min 500 W Xenon lamp Visible light	85%	[38]
BiVO$_4$ 50 mg	ARS 100 ml 100 mg·L^{-1}	180 min 8×8 W low pressure mercury lamp Ultraviolet light	99%	[39]
P25-Ag 50 mg	ARS 100 ml 6.2×10^{-5} mol·L^{-1}	180 min 125 W high-pressure Hg lamp Ultraviolet light	87%	[40]
ZnO 100 mg	ARS 500 ml 25 mg·L^{-1}	90 min UV chamber equipped with seven UV tubes each of 18W Ultraviolet light	77%	[41]
TiO$_2$ 40 mg	ARS 100 ml 0.20 mM	200 min 6-12 phosphor-coated fluorescent lamp (15 W each) Ultraviolet light	99%	[42]
TiO$_2$ 375 mg	ARS 84.2 µmol·L^{-1} 750 ml	120 min high pressure mercury lamp Ultraviolet light	100%	[43]

[19, 20]. In order to apply the photocatalysis technique to practical dye wastewater treatment, it is urgent to explore a photocatalyst that can remove different dyes simultaneously.

Hence, in view of the above-discussed perspective, a new aspect of photocatalytic degradation has been investigated in the current study: the photocatalytic removal efficiency of $TiO_2/H_3PW_{12}O_{40}$ film were evaluated under solar-like radiation for monocomponent dye wastewater – i.e., rhodamine B (RhB), methyl orange (MO), malachite green (MG), and alizarin red (ARS) – together with bicomponent dye wastewater as a mixture of RhB and MG with different volume ratio. The results may provide necessary information on the development of the photocatalysis technique for multiple-component dye wastewater treatment in practical application.

Material and Methods

Catalyst Preparation

The combining process of temperature programming control and the sol-gel-hydrothermal route was employed to prepare for the $TiO_2/H_3PW_{12}O_{40}$ composite film according to our previous studies [12]. The as-prepared film was fabricated with the intact saturation Keggin structure and anatase phase TiO_2 possessing a higher specific surface area (157.9 m²/g), in which actual doping amount of $H_3PW_{12}O_{40}$ was 14.7% [12].

Photocatalytic Experiment

All experiments were carried out in a self-designed quartz reactor (Fig. 1), where $TiO_2/H_3PW_{12}O_{40}$ film (*ca*. 4.5 mg) was immersed in stirring mono-/bicomponent dye solution (120 ml, 25 mg·L⁻¹). For the

four classes of dyes, RhB is a highly water-soluble and cationic alkaline dye of the xanthene class, MO is a representative anion azo dye containing a N=N double bond, MG is a cationic alkaline dye with triarylmethane hydrocarbon derivatives, and ARS is a water-soluble and anion anthraquinone dye widely used as a colorant in textiles. Moreover, LD50 values of dyes are generally

Fig. 4. Ultraviolet-scanning of photocatalytic degradation of RhB-MG binary dye with different volume ratio by $TiO_2/H_3PW_{12}O_{40}$ film.

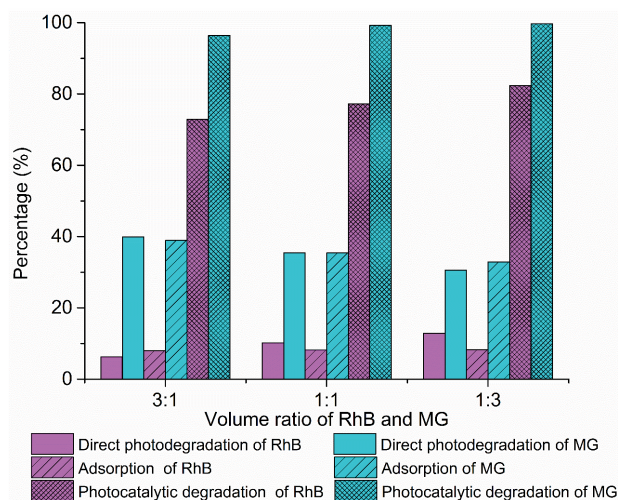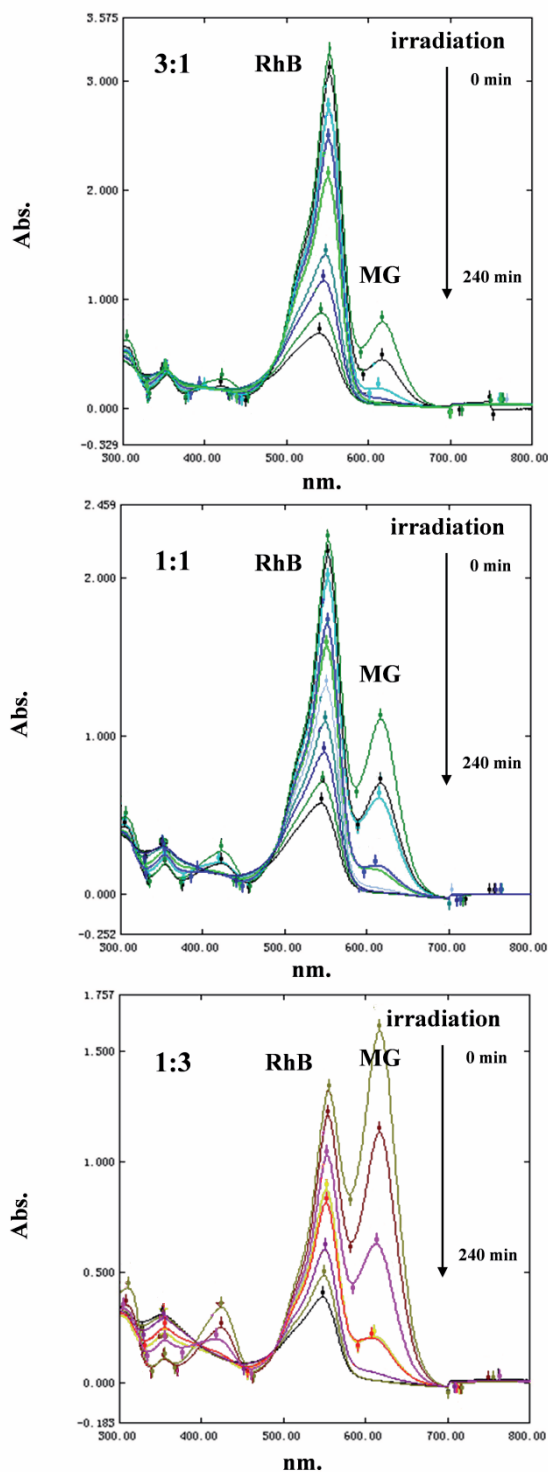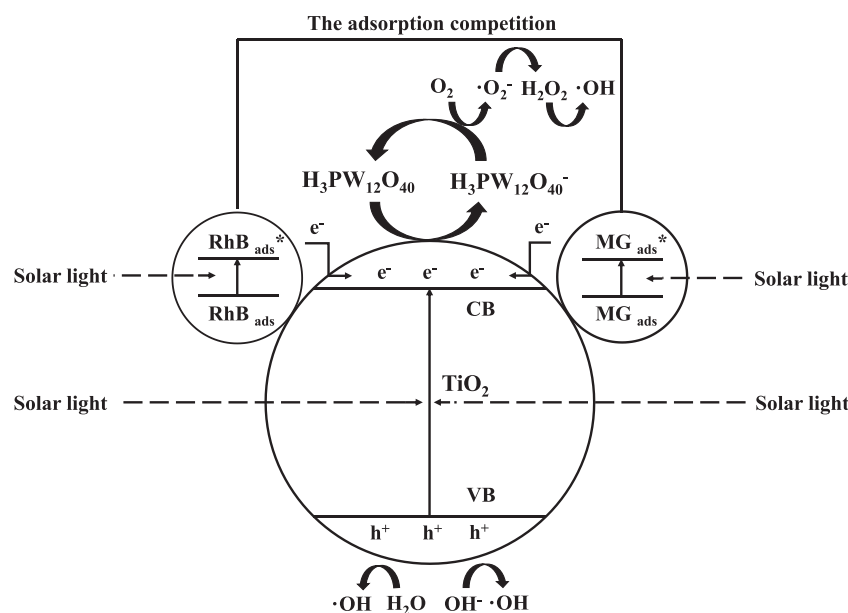Fig. 3. Direct photolysis of RhB-MG composite dye with different volume ratio, and their adsorption and photocatalytic degradation on $TiO_2/H_3PW_{12}O_{40}$ film.

Scheme 1. Photocatalytic degradation mechanism of $TiO_2/H_3PW_{12}O_{40}$-20% film toward RhB-MG composite dye.

greater than 2,000 mg/kg, whereas the alkaline and diazo direct dyes commonly represented lower LD50 values and higher toxicity, as demonstrated by a survey conducted by the Ecological and Toxicological Association of Dyestuff Manufacturing Industry [21]. LD50 values of the dyes selected in the current study are exhibited in Table 1, indicating that they may be toxic even at low concentrations. Additionally, RhB has been classified as a Group 3 carcinogen by the International Agency for Research on Cancer IARC and forbidden to use as a food additive in the United States, European Union, and China; MG also has been banned in several countries, including the United States, Canada, and the European Union. The United States Food and Drug Administration has nominated MG as a priority chemical for carcinogenicity testing. Hence, it is necessary to develop an efficient photocatalysis technique to treat these dye wastewaters, in particular with RhB and MG. Consequently, bicomponent dye solutions were mixed by RhB and MG with different volume ratios (90:30 ml; 60:60 ml; 30:90 ml) to simulate the practical dye wastewater.

First, the mono/bicomponent dye solutions with photocatalyst were stirred for 30 min in order to achieve adsorption-desorption equilibrium. Then the reactor was placed *ca*. 15 cm below a PLS-SXE300 Xe lamp (300 W, Beijing Trusttech Co. Ltd., China) equipped with an IR cut filter to remove most IR irradiation (780-1100 nm). Consequently, the artificial solar light with main emissions from 320 nm to 780 nm matches well with the natural solar light (inset of Fig. 1). The light intensity was adjusted to 200 mW·cm^{-2} measured by a radiometer (OPHIR, Newport, USA). At the given intervals of irradiation, a fixed volume of dye solution was sampled and then analyzed by a Shimadzu double-beam spectrophotometer UV-190 at

λ = 554 nm (RhB), 465 nm (MO), 618 nm (MG), and 424 nm (ARS).

Results and Discussion

Photocatalytic Degradation of Monocomponent Dye (RhB, MO, MG, and ARS)

The direct photolysis of the monocomponent dye solution (120 ml; 25 mg·L^{-1}) and the adsorption on $TiO_2/H_3PW_{12}O_{40}$ film have been investigated (Fig. 2). After 240 min irradiation, the direct photolysis rate of MO was 4.6%, which was much less than that of RhB (24.6%), ARS (40.7%), and MG (51.9%). The adsorption capacity of $TiO_2/H_3PW_{12}O_{40}$ film toward cation dyes (RhB 6.4%; MG 13.6%) was larger than anion dyes (MO 1.3%; ARS 3.2%). The surface of $H_3PW_{12}O_{40}$ in the composite film was negatively charged, resulting in a high adsorption capacity toward cationic dyes rather than anion dyes. Moreover, the enhanced adsorption capacity was agreed with other reports, which can be attributed to the large specific surface area and unique pseudo-liquid phase structure of a Keggin-type $H_3PW_{12}O_{40}$ [22]. The degradation rate reached 98.5%, 95.2%, 89.8%, and 48.8% for RhB, MG, ARS, and MO, respectively, after 240 min solar-like irradiation (Fig. 2). Furthermore, the degradation efficiency of MO was much lower than other dyes due to its chemical structures. The high dissociation energy and less reactivity of MO are attributed to the azo group (-N=N-) and sulfonic group [23]. It is worth noting that even though only an amount of 4.5 mg $TiO_2/H_3PW_{12}O_{40}$ was used in the current system, the degradation efficiency was still considerable in comparison with that in other studies (Table 2).

Table 3 The efficiency of direct photolysis, adsorption and photocatalytic degradation in RhB-MG composite dye system.

Time (min)	RhB:MG = 3:1						RhB:MG = 1:1						RhB:MG = 1:3					
	Direct photolyisis		Adsorption		Photocatalytic degradation		Direct photolyisis		Adsorption		Photocatalytic degradation		Direct photolyisis		Adsorption		Photocatalytic degradation	
	RhB (%)	MG (%)	RhB (%)	MG (%)	RhB (%)	MG (%)	RhB (%)	MG (%)	RhB (%)	MG (%)	RhB (%)	MG (%)	RhB (%)	MG (%)	RhB (%)	MG (%)	RhB (%)	MG (%)
0	0	0	0	0	0	0	0	0	0	0	0	0	0	0	0	0	0	0
30	1.6	7.4	9.6	41.9	16.3	77.3	2.8	7.6	8.7	32.2	11.3	46.0	3.5	5.6	18.1	39.2	17.2	52.6
60	4.1	17.2	9.4	41.9	24.9	89.0	3.5	11.0	8.6	31.9	24.3	83.6	8.7	16.0	18.9	40.8	22.3	62.0
90	4.2	19.5	9.4	42.0	36.0	99.4	4.2	16.2	8.2	32.5	30.8	86.9	9.3	18.3	18.7	39.1	34.3	87.5
120	5.4	27.2	9.1	42.2	48.1	99.6	5.7	21.2	8.7	31.8	42.4	96.5	9.5	19.1	18.0	39.5	38.8	88.7
150	5.5	30.3	9.1	41.5	59.4	99.6	6.3	23.6	8.3	31.7	53.3	98.7	10.4	20.6	18.6	41.1	47.5	95.5
180	6.0	34.0	9.6	42.2	67.4	99.6	6.8	24.6	8.8	32.3	62.2	98.7	11.6	25.8	18.5	40.6	55.7	97.9
210	6.2	38.0	9.8	41.7	76.5	99.6	7.8	30.6	8.7	32.0	70.7	98.9	11.8	27.7	18.4	39.6	64.5	99.2
240	6.3	39.9	9.5	42.1	82.3	99.6	10.2	35.4	8.2	32.8	77.2	99.2	12.9	30.6	18.8	40.7	73.0	99.7

Photocatalytic Degradation of Bicomponent Dyes (RhB-MG)

RhB and MG were selected and mixed on the basis of different volume ratios due to their optimum degradation efficiency in a $TiO_2/H_3PW_{12}O_{40}$ film photocatalytic system. Direct photolysis, adsorption, and photocatalytic degradation of bicomponent dye solution of RhB-MG with different volume ratio were carried out (Fig. 3 and Table 3). The direct photolysis efficiency decreased from 12.9% to 6.3% for RhB and from 39.9% to 30.6% for MG. Owing to a limited overlap of light adsorption for RhB and MG (Fig. 4), the decrease of direct photolysis efficiency was mainly attributed to raise their respective initial concentrations. The adsorption efficiency of RhB was maintained stably in different volume ratios, fluctuating from 8.0% to 8.3%, whereas for MG it increased from 32.9% when RhB: MG = 3:1 (v: v) to 38.9% when RhB: MG = 1:3 (v: v), which indicated that the catalyst processed a higher adsorption affinity for MG in the bicomponent dye solutions. The photocatalytic degradation efficiency of MG was significantly higher than that of RhB, with the efficiency of MG achieving 95.7%, 96.5%, and 88.7% after 120 min irradiation, whereas the degradation of RhB was restrained due to the competition for the active sites of catalyst surface with MG, and the efficiency was only 49.1%, 42.4%, and 38.8%, corresponding to systems of 90:30 ml, 60:60 ml, and 30:90 ml, respectively.

Variations of UV-vis spectra for RhB and MG during the degradation process are shown in Fig. 4. The absorbance peaks were located at 554 nm for RhB and 618 mm for MG. Their intensities decrease with reaction time, indicating the degradation of dyes. Furthermore, the blue shift of RhB and MG peaks did not occur in the system, suggesting that N-demethylation or de-ethylation was not generated during the degradation. However, an intensification of peak at 374 nm was observed, implying the generation of intermediate products through breaking down chromophoric conjugated structure and aromatic rings of the dye comprised of C-C, C=N, or C=C bond. Accordingly, RhB may be degraded into 3-(diethylamino) phenol ($C_{10}H_{15}NO$), 2-(2,5-dihydroxypheny) acetic acid ($C_8H_8O_4$), 2-vinylbenzoic acid ($C_9H_8O_2$), etc. [44], while the intermediate products of MG degradation could be 2-oxosuccinic acid, (E)-4-oxobut-2-enoic acid, or glyoxylic acid [45].

The adsorbed RhB and MG on $TiO_2/H_3PW_{12}O_{40}$ film was excited via absorbing solar light and donated their electrons to the conduction of TiO_2 [46]. At the same time, the electrons were promoted from the valence band to conduction of TiO_2, leaving the holes in its valence band. Afterward, these electrons were scavenged by $H_3PW_{12}O_{40}$, and the generated $H_3PW_{12}O_{40}^-$ reacted with the adsorbed oxygen to produce $\cdot O_2^-$, while $\cdot O_2^-$ would further react with H_2O to form H_2O_2 and ultimately convert to $\cdot OH$. Consequently, the holes

could also react with H_2O or OH^- to form $\cdot OH$. $\cdot OH$ was confirmed as the essential role in the photocatalytic system $TiO_2/H_3PW_{12}O_{40}$ film [46], which could degrade the dyes effectively (Scheme 1). Moreover, the reaction can be driven by the self-regeneration of $H_3PW_{12}O_{40}$ via the redox cycling between $H_3PW_{12}O_{40}$ and $H_3PW_{12}O_{40}^-$.

Conclusion

$TiO_2/H_3PW_{12}O_{40}$ film was applied to photocatalytic degradation of simulated mono- and bicomponent dye wastewater. The results showed that $TiO_2/H_3PW_{12}O_{40}$ film possesses higher adsorption capacity for cationic dyes (RhB and MG) in comparison with anion dyes (MO and ARS) due to the negatively charged surface of $H_3PW_{12}O_{40}$. Despite the competition, a higher photocatalytic degradation of bicomponent dye wastewater was still attained, which suggested $TiO_2/H_3PW_{12}O_{40}$ film may be a potential and efficient catalyst for dye wastewater treatment.

Acknowledgments

Conflict of Interest

The authors declare that they have no competing interests.

References

1. AKPAN U.G., HAMEED B.H. Parameters affecting the photocatalytic degradation of dyes using TiO_2-based photocatalysts: A review. J. Hazard. Mater. **170** (2-3), 520, **2009**.
2. SONG W., GAL B.Y, XING X., XING L.L., HAN S., DUAN P.J., SONG W.C., JIA R.B. Adsorption-desorption behavior of magnetic amine/Fe_3O_4 functionalized biopolymer resin towards anionic dyes from wastewater. Bioresource Technol. **210**, 123, **2016**.
3. MITTAL H., MAITY A., RAY S.S. Gum karaya based hydrogel nanocomposites for the effective removal of cationic dyes from aqueous solutions. Appl. Surf. Sci. **364**, 917, **2016**.
4. SIDDIQUA U.H, ALI S., HUSSAIN T., BHATTI H.N.B., ASGHAR M. The dyeing process and the environment: enhanced dye fixation on cellulosic fabric using newly synthesized reactive dye. Pol. J. Environ. Stud. **5** (26), 2215, **2017**.
5. BHATNAGAR A., SILLANPAA M. Utilization of agro-industrial and municipal waste materials as potential adsorbents for water treatment-A review. Chem. Eng. J. **157**, 277, **2010**.
6. BABUPONNUSAMI A., MUTHUKUMAR K. A review on Fenton and improvements to the Fenton process for wastewater treatment. J. Environ. Chem. Eng. **2** (1), 557, **2014**.
7. NOREEN S., BHATTI H.N., ZUBER M., ZAHID M., ASGHER M. Removal of Actacid Orange-RL dye using biocomposites: modeling studies. Pol. J. Environ. Stud. **5** (26), 2125, **2017**.
8. HINDA L., PUZENAT E., HOUAS A., KSIBI M., ELALOUI E., GUILLARD C., HERRMANN J.M. Photocatalytic degradation of various types of dyes (Alizarin S, Crocein Orange G, Methyl Red, Congo Red, Methylene Blue) in water by UV-irradiated titania. Appl. Catal. B: Environ. **39**, 75, **2002**.
9. CAI Z.L., ZHOU Y.M., MA S.S., LI S.W., YANG H.Y., ZHAO S. Enhanced visible light photocatalytic performance of g-C_3N_4/CuS p-n heterojunctions for degradation of organic dyes. J. Photoch. Photobio. A. **348**, 168, **2017**.
10. FUJISHIMA A., RAO T.N., TRYK D.A. Titanium dioxide photocatalysis, J. Photoch. Photobio. C. **1**, 1, **2000**.
11. SOBCZYNSKI A., DOBOSZ A. Water purification by photocatalysis on semiconductor. Pol. J. Environ. Stud. **10** (4), 195, **2001**.
12. LU N., ZHAO Y.H., LIU H.B., GUO Y.H., YUAN X., XU H., PENG H.F., QIN H.W. Design of polyoxometalate-titania composite film ($H_3PW_{12}O_{40}$/TiO_2) for the degradation of an aqueous dye Rhodamine B under the simulated sunlight irradiation. J. Hazard. Mater. **199-200**, 1, **2012**.
13. RABBANI M., SEGHATOLESLAMI Z.S., RAHIMI R. Selective adsorption of organic dye methylene blue by $Cs_4H_2PMo_{11}FeO_{40}\cdot 6H_2O$ in presence of methyl orange and Rhodamine-B. J. Mol. Struct. **1146**, 113, **2017**.
14. HUANG J., SONG H.Y., CHEN C.X., YANG Y., XU N.D., JI X.Z., LI C.Y., YOU J.A. Facile synthesis of N-doped TiO_2 nanoparticles caged in MIL-100(Fe) for photocatalytic degradation of organic dyes under visible light irradiation. J. Environ. Chem. Eng. **5** (3), 2579, **2017**.
15. NATHALIA P.F., FRANCIELLE C.F.M., ANDRE E.N., ALYSSON S.M., MARCOS R.V.L., ELISABETE M.A. YVAN J.O.A. Hexagonal-Nb_2O_5/Anatase-TiO_2 mixtures and their applications in the removal of Methylene Blue dye under various conditions. Mater. Chem. Phys. **198**, 331, **2017**.
16. KUO C.Y., YANG Y.H. Exploring the Photodegradation of Bisphenol A in a Sunlight/Immobilized N-TiO_2 System. Pol. J. Environ. Stud. **23** (2), 379, **2014**.
17. SINGH P., VISHNU M.C., SHARMA K.K., BORTHAKUR A., SRIVASAVA P., PAL D.B., TIWAR Y., MISHRA P.K. Photocatalytic degradation of Acid Red dye stuff in the presence of activated carbon-TiO_2 composite and its kinetic enumeration. J. Water Proc. Eng. **12**, 20, **2016**.
18. XU X.Y., ZHOU X.S., ZHANG L.L., XU L.M., MA L., LUO J., LI M.J. Photoredox degradation of different water pollutants (MO, RhB, MB, and Cr(VI)) using Fe-N-S-tri-doped TiO_2 nanophotocatalyst prepared by novel chemical method. Mater. Res. Bull. **70**, 106, **2015**.
19. YAGUB M.T., SEN T.K., AFROZE S., ANG H.M. Dye and its removal from aqueous solution by adsorption: A review. Adv. Colloid Interfac. **209**, 172, **2014**.
20. NATARAJAN S., BAJAJ H.C., TAYADE R.J. Recent advances based on the synergetic effect of adsorption for

removal of dyes from waste water using photocatalytic process. J. Environ. Sci. **65**, 201, **2018**.

21. ROBINSON T., MCMULLAN G., MARCHANT R., NIGAM P. Remediation of dyes in textile effluent: a critical review on current treatment technologies with a proposed alternative. Bioresource Technol. **77**, 247, **2001**.

22. LIU C.G., ZHENG T., LIU S., ZHANG H.Y. Photodegradation of malachite green dye catalyzed by Keggin-type polyoxometalates under visible-light irradiation: Transition metal substituted effects. J. Mol. Struct. **1110**, 44, **2016**.

23. ARIYANTI D., MAILLOT M., GAO W. Photo-assisted degradation of dyes in a binary system using TiO_2 under simulated solar radiation. J. Environ. Chem. Eng. **6**, 539, **2018**.

24. HAO Q.M., XU J.Y., ZHUANG X.J., ZHANG Q.L., WAN Q., PAN H.Y., ZHU X.L., PAN A.L. Template-free synthesis and photocatalytic activity of CdS nanorings. Mater. Lett. **100**, 141, **2013**.

25. XIAO K., HUANG H.W., TIAN N., ZHANG Y.H., Mixed-calcination synthesis of $Bi_2MoO_6/g-C_3N_4$ heterojunction with enhanced visible-light-responsive photoreactivity for RhB degradation and photocurrent generation. Mater. Res. Bull. **83**, 172, **2016**.

26. TOLOMAN D., POPA A., STEFAN M., PANA O., SILIPAS T.D., MACAVEI S. Impact of Gd ions from the lattice of TiO_2 nanoparticles on the formation of reactive oxygen species during the degradation of RhB under visible light irradiation. Mat. Sci. Semicon. Proc. **71**, 61, **2017**.

27. LI L., CHENG M., BAI Y., AN B., DANG D.B. A polyoxometalate-based inorganic-organic hybrid polymer constructed from silver-Schiff base building block and Keggin-type cluster: Synthesis, crystal structure and photocatalytic performance for the degradation of rhodamine B. Spectrochim. Acta A. **150**, 846, **2015**.

28. NUENGMATCHA P., CHANTHAI S., MAHACHAI R., OH W.C. Visible light-driven photocatalytic degradation of rhodamine B and industrial dyes (texbrite BAC-L and texbrite NFW-L) by ZnO-graphene-TiO_2 composite. J. Environ. Chem. Eng. **4**, 2170, **2016**.

29. DAI G.P., QIN H.Q., ZHOU H., WANG W.Q., LUO T.X. Template-free fabrication of Hierarchical macro/mesoporous SnS_2/TiO_2 composite with enhanced photocatalytic degradation of Methyl Orange (MO). Appl. Surf. Sci. **2017** [In press].

30. KUMAR R., KUMAR G., UMAR A. ZnO nano-mushrooms for photocatalytic degradation of methyl orange. Mater. Lett. **97**, 100, **2013**.

31. ZHANG L., ZHAO Y., ZHONG L.L., WANG Y., CHAI S.N., YANG T., HAN X.L. $Cu_2S-Cu-TiO_2$ mesoporous carbon composites for the degradation of high concentration of methyl orange under visible light. Appl. Surf. Sci. **422**, 1093, **2017**.

32. WANG Y.Z., ZHONG M.Q., CHEN F., YANG J.T. Visible light photocatalytic activity of TiO_2/D-PVA for MO degradation. Appl. Catal. B: Environ. **90**, 249, **2009**.

33. GHIASI M., MALEKZADEH A. Solar photocatalytic degradation of methyl orange over $La_{0.7}Sr_{0.3}MnO_3$ nano-perovskite. Sep. Purif. Technol. **134**, 12, **2014**.

34. AFSHAR S., JAHROMI H.S., JAFARI N., AHMADI Z., HAKAMIZADEH M. Degradation of malachite green oxalate by UV and visible lights irradiation using $Pt/TiO_2/SiO_2$ nanophotocatalyst. Sharif Uni. Technol. **18**, 772, **2011**.

35. LIU Y., OHKO Y., ZHANG R., YANG Y., ZHANG Z. Degradation of malachite green on Pd/WO_3 photocatalysts under simulated solar light. J. Hazard. Mater. **184**, 386, **2010**.

36. SAIKIA L., BHUYAN D., SAIKIA M., MALAKAR B., DUTTA D.K.D., SENGUPTA P. Photocatalytic performance of ZnO nanomaterials for self-sensitized degradation of malachite green dye under solar light. Appl. Catal. A: Gen. **490**, 42, **2015**.

37. MAGDALANE C.M., KAVIYARASU K., VIJAYA J.J., JAYAKUMAR C., MAAZA M., JEYARAJ B. Photocatalytic degradation effect of malachite green and catalytic hydrogenation by UV-illuminated CeO_2/CdO multilayered nanoplatelet arrays: Investigation of antifungal and antimicrobial activities. J. Photoch. Photobio. B. **169**, 110, **2017**.

38. BAGHDADI M., SOLTANI B.A., NOURANI M. Malachite green removal from aqueous solutions using fibrous cellulose sulfate prepared from medical cotton waste: Comprehensive batch and column studies. J. Ind. Eng. Chem. **55**, 128, **2017**.

39. ABRAHAM S.D., DAVID S.T., BENNIE R.B., JOEL C., KUMAR D.S. Eco-friendly and green synthesis of $BiVO_4$ nanoparticle using microwave irradiation as photocatalyst for the degradation of Alizarin Red S. J. Mol. Struct. **1113**, 174, **2016**.

40. MICHELE L., SOUZA D., CORIO P. Effect of silver nanoparticles on TiO_2-mediated photodegradation of Alizarin Red S. Appl. Catal. B: Environ. **136-137**, 325, **2013**.

41. KANSAL S.K., LAMBA R., MEHTA S.K., UMAR A. Photocatalytic degradation of Alizarin Red S using simply synthesized ZnO nanoparticles. Mater. Lett. **106**, 385, **2013**.

42. DEL G.T., GERMANI R., SARACINO F., STRADIOTTO M. Counterion effect of cationic surfactants on the oxidative degradation of Alizarin Red-S photocatalyzed by TiO_2 in aqueous dispersion. J. Photoch. Photobio A. **332**, 546, **2017**.

43. LACHHEB H., PUZENAT E., HOUAS A., KSIBI M. Photocatalytic degradation of various types of dyes (Alizarin S, Crocein Orange G, Methyl Red, Congo Red, Methylene Blue) in water by UV-irradiated titania. Appl. Catal. B: Environ. **39**, 75, **2002**.

44. DIAO Z.H., LIU J.J., HU Y.X., KONG L.J., JIANG D., XU X.R. Comparative study of Rhodamine B degradation by the systems pyrite/H_2O_2 and pyrite/persulfate: Reactivity, stability, products and mechanism. Sep. Purif. Technol. **184**, 374, **2017**.

45. LIN Y., WU S.H., LI X., WU X., YANG C.P., ZENG G.M., PENG Y.R., ZHOU Q., LU L. Microstructure and performance of Z-scheme photocatalyst of silver phosphate modified by MWCNTs and Cr-doped $SrTiO_3$ for malachite green degradation. Appl. Catal. B: Environ. **227**, 557, **2018**.

46. LU N., LU Y., LIU F.Y., ZHAO K., YUAN X., ZHAO Y.H., LI Y., QIN H.W. $H_3PW_{12}O_{40}/TiO_2$ catalyst-induced photodegradation of bisphenol A (BPA): Kinetics, toxicity and degradation pathways. Chemosphere **91**, 1266, **2013**.